

# Hiding in plain sight: observing objects in low lunar orbit and the L2 dark cone from a lunar surface observatory

Jeffrey E. Van Cleve, Anna Lawitzke, Emily MacAnlis, Jacob D. Griesbach, Melissa Sampson, David P. Osterman, Elvis D. Silva, Christopher J. Grant, and Amelia Bloom  
*Ball Aerospace, Colorado*

## ABSTRACT

While a high-performance sensor at EML-1 could surveil the key orbital trajectories in Earth-Moon space, Low Lunar Orbit (LLO) would remain a challenging subdomain in which to identify unknown objects or detect maneuvers and configuration changes. In addition to the phase angle disadvantages in common with the rest of cislunar space, objects in LLO can be hidden by straylight when near the lunar limb, passing in front of the lunar disk, or obscured by the Moon itself in a conical volume between the Moon and EML-2. We explore the pros (and cons) of a smallsat-scale Lunar Surface Observatory (LSO) as an adjunct to a high-performance L1-based sensor or cislunar constellation, delivered to the lunar surface by commercial lunar payload service (CLPS) providers vetted by NASA. We consider

- Astrodynamics, coverage, and radiometry of objects in regions hidden from EML-1
- Incremental deployment of a network of several stations, starting with an initial operational capability (IOC) of a south polar station with persistent solar illumination and Earth LOS for comm
- Site selection methodology using Lunar Reconnaissance Orbiter (LRO) VIS, IR, and LIDAR maps
- A Wide Field of View (WFOV) camera derived from the Ball CT-2020 star tracker
- A related Fisheye camera pointing at zenith to detect nearby and rapidly moving objects
- Ball dust mitigation and dry lubrication technology to protect optics, solar panels, and moving parts
- Moon-unique thermal engineering experience learned in our L-CiRIS thermal imaging camera to be delivered to the lunar S pole in 2023
- Lunar surface delivery as a commercial product by vendors pre-approved by NASA
- Instrument suites grouping charged particle, RF, and other payloads with the cameras to which together accomplish a mission
- Bonus science: levitating lunar dust, pathfinder for large electro-optic or infrared (EOIR) lunar observatories for astronomy

## 1 Introduction: Exploration of Cislunar Mission Space

### 1.1 Overview

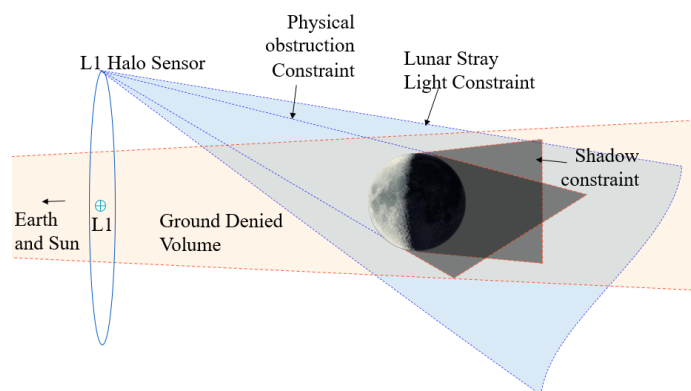


**Figure 1-1: Schematic Earth and L1 access constraints near the Moon near full Moon. The LSO can help increase visible access to low lunar objects as well as the obscured cones. See Figure 1-3 for scale drawing.**

Over the last few years, as many nations and private enterprises develop and execute missions in cislunar space and on the lunar surface, there has been a substantial amount of new activity related to the development of cislunar Space Domain Awareness (SDA) concepts and architectures. One of the primary challenges identified is a cislunar SDA architecture that performs well from a traffic management and awareness perspective over the vast volume and diverse dynamical and lighting conditions of this region. Existing space-based and earth-based architectures have constraints on their observable volumes, including solar and lunar exclusion angles for sensors. While the Moon is not bright enough to damage sensors, it is still bright enough to make faint sources near lunar limb undetectable, and of course blocks objects behind it and renders

objects in front of it difficult to discriminate, as shown in **Figure 1-1**.

Over that same period, Ball Aerospace has evaluated various concepts to address the question of cislunar SDA. Studies by Silva et al. [1] identified options and established a pareto-optimal front for heterogeneous architectures in cislunar space. Those assessments have enabled Ball to establish a high-dimensional space of architecture options, iterative dimensionality control, and an impartial approach to sensor architectures before commitment to particular solutions. In this assessment, we weigh the value of using sensors on the lunar surface to aid in filling the gap in cislunar SDA for objects that are close to or behind the moon. The mission analysis uses a telescope design optimized for detection of dim objects and establishes a proposed set of requirements for a sensor to meet relevant mission need.

Our benchmark target for these assessments is a 1-m diameter Lambertian sphere of 20% albedo. Performance is assessed against a deck of benchmark targets in lunar orbits representing lunar mapping, landing approach, or Non-Rectilinear Halo Orbits (NRHO) [2] approximated as large Elliptical Lunar Orbits (ELOs). We will focus on broadband visible-wavelength (400 nm – 900 nm) optical sensors in our mission analysis though the observatory may have other instruments.

## **1.2 Elements of the LSO System**

The LSO system is composed of an LSO Network on the lunar surface and support elements such as relay satellites, ground stations, and data processing and distribution. The LSO Network has one or more observatories. An observatory includes an instrument suite, and a bus which provides infrastructure like communications, power, structure, data handling (including crypto) and gross thermal control. An observatory is a payload from the lunar lander provider's point of view, but some bus functions may be provided by the lander. The location of an observatory is its "station," in line with evolving IAU naming rules (for example, the Chang'e 4 site is Statio Tianhe). The instrument suite (§ 5.1) is composed of Electro-Optical (EO), RF, particles and fields, PNT (position, navigation, and timing), and other instruments which together perform the domain awareness mission. Instruments provide their own pointing control, if needed, as well as fine thermal control.

## **1.3 The Hidden Zone Close to the Moon**

While the "cone of shame" near the Sun is the *bête noire* of ground-based SDA, there is a similar zone near the Moon which we define in this section for straylight (both telescope and atmospheric) and geometric obstruction. These limits define the volume over which LSO is required to search, while leaving the rest of the vast cislunar domain to larger sensors and orbiting platforms better suited to the task of deep space surveillance. The straylight results will also be applied in a companion paper in this conference [1] to define the minimum angle between telescope boresight and the lunar limb while performing the SDA mission.

### **1.3.1 Straylight in Space Telescopes**

Straylight analysis is a subfield of optical engineering unto itself, and cannot in general be treated with physics approximations. Detailed design information, down to the level of fasteners and the angular and wavelength properties of coatings, is required to quantify straylight from very bright sources well away from the optical axis. However, to illuminate some of the design issues, and set some physics-based limits on how close to the Moon we might look for faint sources using space telescope, we can approximate straylight near the telescope axis as being dominated by that from the Primary Mirror (PM), with these components:

- Small-angle scattering from surface roughness and medium-frequency figure errors, the Bidirectional Reflectance Distribution Function (BRDF)
- Isotropic (Lambertian) scattering from dust
- Diffraction from the aperture, of diameter  $D$

**Table 1-1: Example Telescope for Straylight Calculation**

Baffle Length (L)	900	mm
Baffle Diameter (D0)	300	mm
Mirror Diameter (D)	300	mm
focal length (f)	600	mm
Mirror BRDF Constant (b)	1.00	
Mirror BRDF Slope (m)	-2.23	
Pixel Pitch (s)	0.018	mm
IFOV	6.18	arcsec
$\lambda$	0.75	$\mu\text{m}$
Lambertian Scattering	1.0%	

The simplest method of avoiding straylight is to increase the telescope baffle tube length L so that light from objects more than  $\tan^{-1}(D/L)$  degrees off-axis do not illuminate the PM at all; however, the telescope moment of inertia increases rapidly with L and we take  $L/D \sim 3$  is a practical limit. Likewise, mirror cleanliness and figure precision have practical limits. Aperture diffraction can be suppressed by pupil apodization, at the expense of broadening the central peak of the diffraction pattern.

Since the design of a straylight-optimized space telescope for viewing faint objects near the Moon would be another AMOS paper, we will suggest a “reasonably-well baffled telescope” to calculate how close to the Moon we can look, with the parameters in Table 1-1.

We calculate the Point Source Transmission (PST) at the center of the FOV from a stray light source an angular distance  $\alpha$  from the boresight, using:

- The BRDF equations [3] with typical visible-light BRDF constants. Similar values can be deduced from a nice worked example by the Cerro Tololo Inter-American Observatory [4] (after some units conversion)
- Angle independent Lambertian scattering = (Power on PM)\*(scattering fraction)/ $4F^2$ , where  $F$  = F-number
- Diffraction straylight derived from [5]

$$PST_D = \frac{4(1 + \epsilon)}{\pi^3(1 - \epsilon^2)^2DF^2\alpha^3}$$

Where  $\epsilon$  is the central obscuration. The PST is converted to the Point-Source Rejection Ratio (PSRR) by multiplying by  $(s/D)^2$  where s is the pixel pitch, and converted to a magnitude difference, where the PSRR is the brightness of the straylight in a single pixel divided by the total flux from the straylight source. Since the magnitude of the full Moon as seen from Earth and approximated as a point source is -12.7 and that of the reference target at the Earth-Moon difference is 19.9, a PSRR of 32.6 magnitudes means that lunar straylight is equal to the target flux in a pixel, in the limiting case that most of the target flux is in a single pixel (streaking targets make the problem worse). Targets fainter than the straylight can be observed, at the cost of proportionately longer integration times, until systematic errors become difficult to remove at a straylight/target flux per pixel  $\sim 20$ , or a PSRR of 29.3 mag.

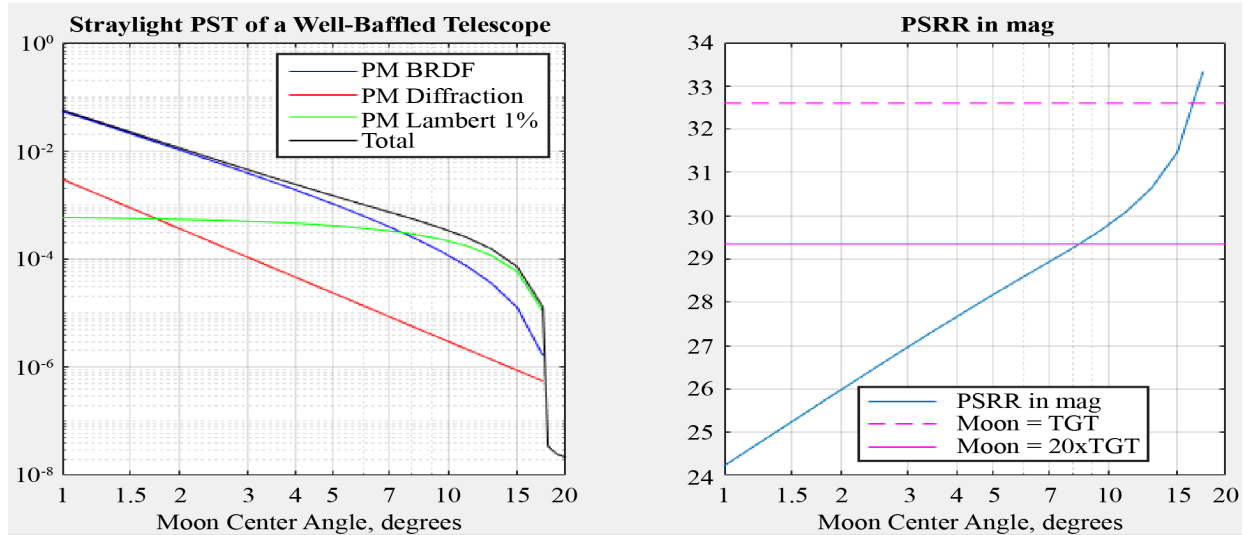


**Figure 1-2: Near-boresight Full Moon Straylight for a Well-Baffled Telescope. The Moon Center Angle is the distance between the target and the center of the lunar disk. TGT = target.**

The left panel of **Figure 1-2** shows the relative contributions. Note that diffraction falls off somewhat more rapidly than BRDF, and that BRDF and Lambertian fall off beyond 10 degrees as less and less light is incident on the PM, becoming insignificant at 18 degrees (outside the range of interest and of the validity of the approximation). The right panel shows the PSRR limits. The angular limit (8.1 degrees) is to a first approximation independent of distance to the Moon and lunar phase if a) both the Moon and target are approximated as Lambertian spheres and b) the observer is near the Earth-Moon line and c) the target and Moon are about the same distance to the observer. Then Moon and

target fluxes scale the same with phase and distance. Of course, the when the observer is closer to the Moon the straylight limit in km is lower, and positing a “reasonably well-baffled” observer at EML1 gives us a limiting altitude of 6500 km above the lunar surface as the outer limit of the search volume for LSO.

Modeling the Moon as an extended source does not fundamentally change these conclusions for observers further from the Moon than EML1 (58,000 km). Obviously, the LSO itself is on the Moon’s surface and violates this simple scaling rule, so a simple criterion of “keep the Moon off the PM” will inform the baffle design (S 2.2). The EML1 observer limits are shown in red in **Figure 1-3**.

### 1.3.2 Sky Brightness near the Moon at Night for Earth-based Observers

Ground-based observatories are possible elements of a comprehensive cislunar SDA architecture of which LSO is also an element, so we examine the moon angle limits for ground-based observers. Krisciunas and Schaefer [6] modeled the sky brightness of moonlight – a form of straylight if one considers the atmosphere as part of the optical system -- at Mauna Kea (an excellent site). We extended the results shown in Table 2 [6] by:

- interpolating for  $5 < \alpha < 30$  degrees
- scaling as  $1/\alpha^2$  for a  $< 5$  degrees
- scaling the result for 30-degree phase angle  $\phi$  to 0 degrees (full Moon) by subtracting 1.0 magnitudes
- scaling as  $1/\lambda^4$  for Rayleigh scattering (that is, adding  $10 \cdot \log_{10}(\lambda/\lambda_{VIS})$  in magnitude limits)

We take an IFOV of 1.0 arcsec as a good compromise between resolution (seeing  $< 0.25$  arcsec at Mauna Kea) and FOV (3 x 3 degrees) for reasonable ground-based array sizes (10.8 kpix x 10.8 kpix). Most SDA systems are panchromatic visible light (centered on astronomical V-band), but as a bounding case we also looked at the near-infrared H band because of the Rayleigh law. We did not consider K band, the next longer atmospheric window, since the solar spectrum and hence reflected signal from targets starts to decline between H and K. We found that the systematic error limit (straylight = 20x target in pixel) is 13.3 degrees from the center of the Moon or 87,000 km altitude for a V-band imager, and 0.75 degrees from the center of the Moon or 3300 km altitude for an H-band (1.65  $\mu\text{m}$ ) imager, each with 1.0” pixels. **Figure 1-3** shows the region persistently hidden from this hypothetical H-band imager network in gold, with a diverging 0.75 degree half-cone on the near side of the Moon and a converging 0.75 degree half-cone on the far side. This converging half-cone is due to diurnal parallax; Earth-based observers can “look behind” the Moon a little near Moonrise and Moonset.

### 1.3.3 Geometrical Obstruction

Objects transiting the lunar disk are hidden in a cone with the tip at the observer and the base subtending the lunar disk, while objects are occulted by the lunar disk in the extension of this cone to infinity. For observers which move in the EMRF, such as (non-polar) observers on the rotating Earth or observers in orbit around the Earth or a Lagrange

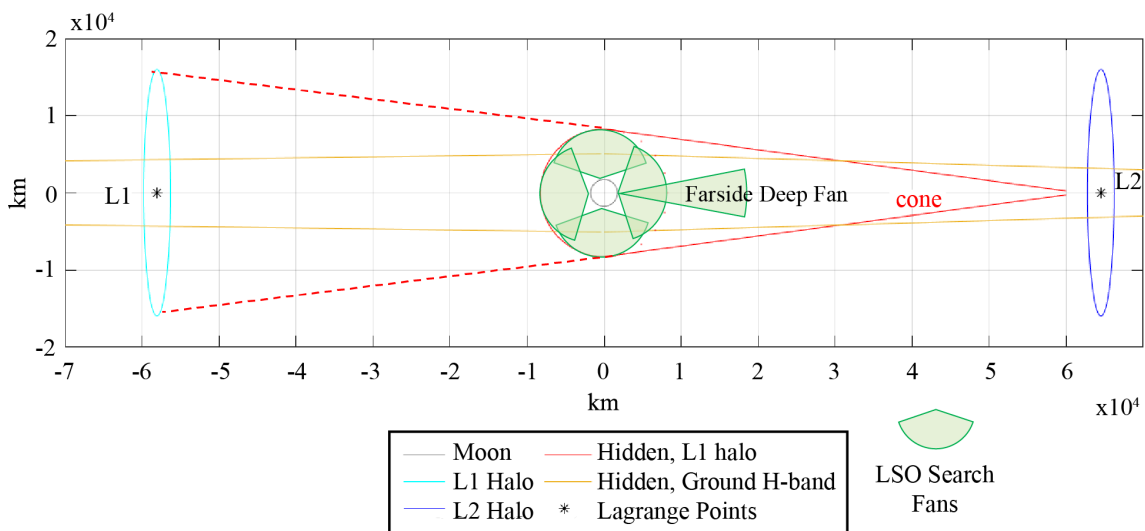


**Figure 1-3: Scale Drawing of Zone near the Moon Hidden from L1 and Earth-based observers, with LSO search fans discussed in the text. Note the entire region is inaccessible to ground-based VIS systems. The H-band cone tapers beyond the Moon because of the parallax of the Earth’s rotation.**

point, we consider the hidden cone to the intersection of these instantaneous transit and occultation cones. These transit and occultation regions are small compared to the straylight-excluded regions discussed above, but are particularly refractory since they persist no matter how bright the target, or how good the PSRR.

**Figure 1-3** combines the results in this section, showing the hidden zone for a well-baffled L1 halo telescope and a hypothetical 100 Mpix H-band (1.65  $\mu\text{m}$ ) camera which exploits the  $1/\lambda^4$  scaling of Rayleigh scattering and the ability to field much larger focal plane arrays on the ground at the same cost. However, such an H-band camera would be unavailable >65% of the time due to daylight, proximity of the Moon to the Sun, rotation of the Earth, and weather. Note that building and operating 3+ 100 Mpix H-band imagers on meter-class telescopes, distributed around the world in longitude, is in itself a major project.

## 2 Exploring Hidden Zone Solutions

In this section we present an example of exploring the high-dimensional space of architecture options with modest resources, using iterative dimensionality control: vary some dimensions slowly (the outer loop of a complete concept space search), optimize over others (“fast dimensions,” or inner loops of a concept space search), interpret the results with some simple geometry and semianalytic models, then modifying the slow-varying dimensions and repeat. In this study, the slow dimensions were chosen to be telescope parameters, locations on the lunar surface, and target deck, while the fast dimensions were solar vs. nuclear, relay vs. direct LOS to Earth, and one S. Polar station vs a 5-station network with  $4\pi-\epsilon$  coverage at the radial limit of the search volume.

### 2.1 Assumptions and Boundary Conditions

#### 2.1.1 NASA Examples: CLPS Delivery and PRISM Instruments

Currently, most US science and exploration deliveries to the Moon are done through NASA or a NASA Commercial Lunar Payload Services (CLPS) provider [7]. The CLPS providers offer commercial delivery where companies can procure space and a ride to the lunar surface. There are several international companies, such as i-space, also looking to provide lunar surface deliveries. CLPS missions deliver scientific instrument suites through the PRISM [8] program, which allocates mass, power, comm, and cost to the suites. We will use CLPS and PRISM as examples throughout this paper.

Current landed costs per kilogram are significantly higher than to other orbits, as the published cost from Astrobotic [9] is \$1.2M/kg of payload delivered to the lunar surface, while the advertised (booster reuse) fare for SpaceX insertion into GTO is about \$12,000/kg for Falcon 9 [10]. This is not surprising, as having a payload delivered to the lunar surface with a soft landing requires a much more robust vehicle and controls than a satellite or satellite bus. As deliveries to the lunar surface increase, price is expected to decrease. This is analogous to the price decrease in the satellite-as-a-service market or space-as-a-service market. Multiple companies are providing hosted/condo/rideshare payload opportunities and prices are competitive. Customers have many commercial companies to choose from with a wide variety of amenities, such as power, orbit, communications, etc. This allows payloads to focus on the payload purpose and eliminates the need for every payload to be self-sufficient with life support systems, such as propulsion, communications, hardware, etc.; these life support systems are provided as part of the service the payload customer purchases. But the bottom line remains, since soft-landing a payload on the Moon is  $\sim 100\times$  the cost/kg of inserting that payload into GTO, it is important to choose LSO’s scope wisely to do what it does best: watch near-lunar space.

#### 2.1.2 Power and Comm

The most critical decisions about a lunar lander architecture is whether the system is expected to operate throughout the lunar night, and whether there is a comm relay providing near-constant link to Earth.

One of the challenges of being a hosted payload on a CLPS provider is there is currently no CLPS provider offering lunar night survival and multi-month operations, though some “few hours after sunset” scenarios are being investigated. Night survival options are being discussed in the CLPS community, so the LSO duty cycle could be close to 50%. For night operations, nuclear power, in the form of Radioisotope Thermal Generators (RTGs), has of course been around since the 1970’s for outer Solar System missions and is in current use on the surface of Mars. RTGs have been revived by renewed production of Pu-238 and a decrease in vocal public opposition since the late 90’s. However, they are very heavy and expensive compared to solar power, with a specific power of 2.67 W/kg (after fueling, declining 1%/year thereafter [11]) and specific cost of \$1.0 M/We [12], to which must be added the \$1.2 M/kg delivery charge to the lunar surface. A third option is solar power beaming [13] on the surface of the Moon, which could be utilized to provide continuous power to an LSO. For polar LSOs near a peak of persistent light, solar power can be beamed to the LSO directly from collectors just a few km away. More generally, power could be beamed from

orbit to surface stations or power relays. Since the beaming concept is still being developed while many RTGs have been built and flown, we do not attempt to consider cost-effectiveness for beamed power systems.

The most primitive communication method is Direct-With-Earth (DWE) in which comm occurs only when the Earth is above the horizon. This is exceedingly unsatisfying, since polar stations would be out of touch half the month at a time, while Farside stations would not work at all. Persistent and pervasive lunar surface operations will require a comm relay network. A 100% available comm relay network would consist of a minimum of two space vehicles in phased Lagrange halo orbits or Non-Rectilinear Halo Orbits (NRHOs) to enable operation on the Farside and at polar stations for which DWE is poor or nonexistent. However, an initial operating capability for relay could be NASA's Lunar Gateway, which would be available as a relay to a S. Polar station over 86% of the time [2] or more (this work) at low marginal cost. Buildout to the 5-satellite relay constellation envisioned by NASA's LunaNet [16], which would prove near-continuous and global access, could occur over the subsequent decade.

We will compare effectiveness vs. cost for solar vs. nuclear and look at the effectiveness of an Initial Operating Capability (IOC) of a single station on the rim of Shackleton crater which lands before a relay network becomes fully operational. However, there are no scenarios with a large amount of activity at the lunar poles or Farside which do not have a comm relay network; indeed, a lunar comm relay already exists in the form of Queqiao, which relayed data from the Farside Chang'e 4 lander and its rover back to China. So we do not analyze multi-station scenarios with no comm relay.

### 2.1.3 Locations on the Moon

In order to keep down the dimensionality of our study, we choose a S. Polar site because of its proximity to the nexus of human activity over the next decade or more. We then distributed around the Moon the minimum number of stations which together can view  $4\pi$  around the Moon each with Fields of Regard (FOR) somewhat less than  $2\pi$ : one North Polar site, and 3 equatorial sites. The equatorial sites are located so that two of them have LOS to Earth at  $\pm 60$  degrees longitude, and the other is located on the center of the Farside.

## 2.2 Wide Field-of-View (WFOV) Camera Requirements and Radiometry

Telescope design is tightly coupled to mission design, an obvious example being the relationship between target flux, FOV, FOR, IFOV, revisit time, and required SNR. Design considerations include telescope diameter  $D$ , pupil area  $A = (\pi D^2/4)$ , and the solid angle  $\Omega$  of the FOV. Typically, large telescopes have small  $\Omega$  and small telescopes can have larger  $\Omega$ , with  $A\Omega$  or 'etendue' being an informal measure of optical difficulty. For efficient observing, the telescope must also spend most of its time collecting photons instead of slewing and settling. Since moments of inertia scale as the fifth power of linear dimension, big telescopes are hard to move quickly and also typically cost more as roughly  $D^2$ . The optimal design is typically a compromise between a telescope that's too small to cover the FOR in the revisit time and one that's too big to be efficient in cost or observing time. The mission also pushes in the direction of larger IFOVs, since a given number of pixels can cover more of the sky if the IFOV is bigger, subject to an upper bound based on available physical pixel size and the metric accuracy requirement for target location in the image – bigger IFOVs mean larger angular errors for a given centroiding error.

To anchor the mission analysis in the next section, we consider a telescope using these first-order requirements:

1. SNR  $\geq 6$  on the benchmark SDA target at 90-degree phase angle 6,500 km (the fan depth derived in S 1.3.1. The benchmark target thus has visual magnitude  $m_v = 12.3$ .
2. A FOR of half-angle 80 degrees, so the sky above 10 degrees elevation can be seen with the 10 degrees an upper bound on local topography and lander tilt angle.
3. Achieve the SNR of Requirement 1 while sweeping the FOR in half the period of the lowest stable lunar orbit (half of 108 min = 54 min).

Subject to these assumptions and evaluation criteria:

1. The wavelength range is panchromatic VIS, 400-900 nm.
2. The effective F/# is  $>2.0$  for to constrain the complexity of the optical design, where the effective F/# combines the F/# of a point source and the width of the FOV.
3. The focal plane properties are similar to the ON Semiconductor STELLAR-III, with pixel pitch is 12.8 microns, read noise is 30 e- and independent of integration parameters, and dark current is negligible. Focal plane properties are "sticky" in the sense that one typically picks existing space-qualified focal planes for a first-order analysis, rather than having focal plane requirements as an output, since it is costly and uncertain to redesign, test, and requalify a focal plane. Other vendors, such as Teledyne, have similar products.
4. The signal is described as White Gaussian Noise (WGN).

These requirements and assumptions lead us to a general solution of telescopes with an  $A\Omega$  product  $> 500 \text{ cm}^2\text{deg}^2$ , where  $A$  is the aperture area and  $\Omega$  is the solid angle subtended by the Field of View (FOV). Telescopes with larger apertures typically have smaller FOVs but can reach an SNR threshold in less time. Size is limited by telescope agility, which degrades performance when the telescope spends less time gathering photons than in moving from one place on the sky to another.

### 2.3 Example WFOV Solution: CT-2020 Star Tracker-based Camera

We can keep down the dimensionality of this study by not extensively exploring telescope design space, but by selecting designs that have been produced for flight. One example is the Ball CT-2020 star tracker shown in **Figure 2-1**, which has an aperture of 34 mm and FOV of  $10 \times 10^\circ$ , giving an  $A\Omega$  product of  $1000 \text{ cm}^2\text{deg}^2$ , twice that of the requirement. The pixel size is 35.2 arcsec or  $171 \mu\text{rad}$ . If mounted on an agile gimbal, would collect data for 5 s ( $5 \times 1.0 \text{ s}$  frames), then slew and settle for 3 s, and thus sweep the FOR in 22 minutes. The CT-2020 uses the flight-qualified STELLAR CMOS  $1024 \times 1024$  focal plane array from ON Semiconductor as per our radiometric axioms.

With this WFOV camera, we can also search the L2 dark cone using longer integration times and averaging more

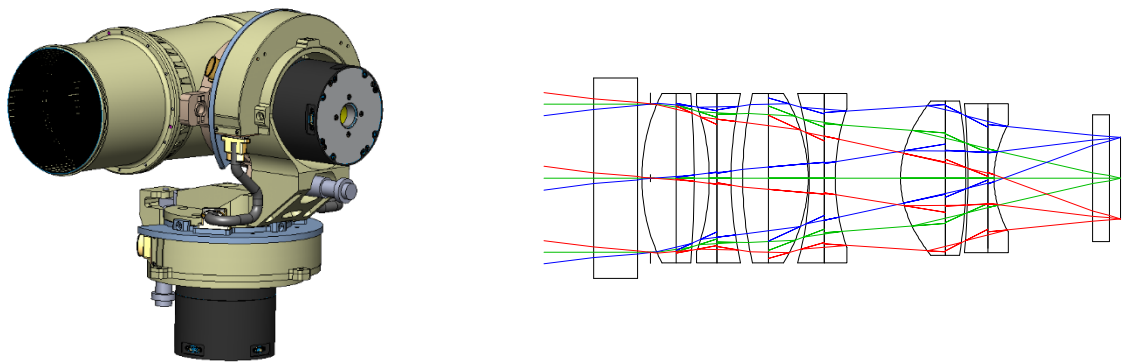


**Figure 2-1: WFOV camera, based on Ball CT-2020 star tracker, on two-axis gimbal (left) provides SDA coverage of the Hidden Zone with optics giving a wide FOV and broad wavelength coverage (right).**

frames (6 s integration time per frame, 32 frames) to reach a range of 14,000 km over the fan marked as “Farside Deep Fan” in **Figure 1-3**. Ball data on the STELLAR focal plane data shows that dark noise scales as expected for these integration times and number of frames. Since the tip of the dark cone is 60,000 km away, we will consider a larger telescope for the Farside site in future studies, and whether other architecture elements can cover this volume [1].

### 2.4 Devil in the Details: Second Order Sensor Properties

It is very important to note that these first-order parameters are not sufficient for good operational performance. Not all 3.4 cm telescopes are alike: quality, as well as size, matters.

- The image must not be smeared more than half a pixel during an integration by telescope jitter and drift. This is one of the historical justifications for lunar observatories – the Moon is a solid platform from which to observe, and in addition rotates so slowly ( $0.55^\circ/\text{s}$ ) that sidereal tracking is not needed for medium-sized pixels and short integration times such as we have. We support this with a robust gimbal concept to “point and shoot” – no tracking of moving targets or the sidereal frame.
- The telescope must be agile, so that the time spent slewing and settling is small compared to the amount of time collecting photons.
- Excellent straylight control is required to observe objects close to the lunar horizon (10 degrees or so at the edge of the FOR), so surface light doesn’t bounce off optics and baffles and into the focal plane. **Figure 2-1** shows a design well-baffled for  $30^\circ$  off-axis, with longer baffles as an option in future studies to get good straylight rejection down to  $10^\circ$ .

### 2.5 Seeing Low-Flying Objects is Hard

Some simple geometry shown in **Figure 2-2** suggests that a WFOV will have a low probability of detecting objects close to the lunar surface. First, the FOR cones subtend a smaller and smaller fraction of the isoaltitude sphere as the altitude gets lower. Second, the angular rate of objects crossing the FOR is inversely proportional to their altitude, and at some point, low-flying objects will pass entirely through the FOR in much less time than the 22 minutes required to sweep the FOR. This simple model estimates that it will be difficult to see targets below 160 km more than once

per day on the average for the 5-station network (§ 2.1.3), while targets above one lunar radius in altitude will be observed at least twice per target orbit. This conjecture is supported by the detailed WFOV mission modeling in § 3.1. In addition, landing craft will of course be at 20 km or less [14] and it would be of interest to observe their descent even if their arrival is unannounced.

This suggests the need for an Ultra-Wide FOV (UWFOV) or “Fisheye” camera pointed at zenith which does not move, continuously watching almost a hemisphere like a meteor or aurora camera. Fortunately, objects close enough to cause a problem are exceedingly bright –  $m_v = 1.7$  for the reference target passing 50 km overhead -- so the camera aperture can be a few mm, keeping the  $A\Omega$  product (a proxy for optical design difficulty) the same as that for the WFOV camera.

### 2.6 Fisheye Camera Requirements and Bounding Concepts

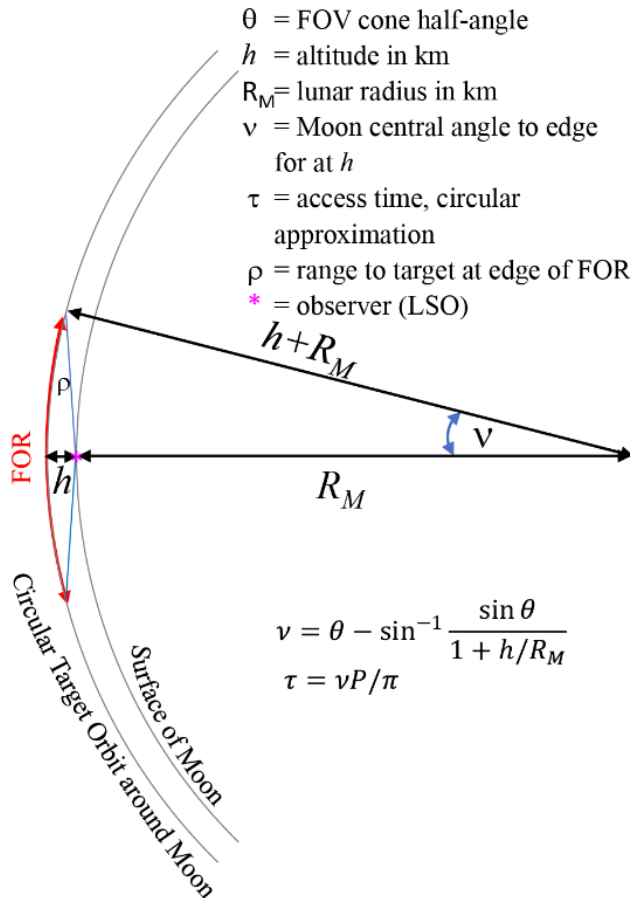


**Figure 2-2: Low-Flying Objects will be hard to see in a WFOV Camera on the surface of the Moon.**

provides hemispherical coverage but narrow spectral bandpass designed by Nikon Patent USPT 3,737,214, while the second is a variation on a Ball heritage more panchromatic 90° diameter lens. The comparison shows the substantial first lens size difference that the smaller FOV enables. A future trade study of a single 128° diameter FOV camera vs. 3 or 4x 90° diameter FOV cameras will depart from these bounding cases to optimize SWaP and cost. Multiple, smaller FOV cameras can also be aimed to avoid other lander instruments and appendages in the joint FOV. An example of this kind of study is the TESS exoplanet mission, which uses 4 nearly identical cameras which together to view a large solid angle of sky [15].

Following **Figure 2-2**, it is desired that the Fisheye FOV equal the WFOV FOR for complete overlap. However, we are confident we can design a somewhat smaller FOV – 64° radial, or 128° diameter – as we did for the ASIMA mission proposal [32] and another program at Ball, and adopt this as the requirement. 128° diameter FOV falls midway between designs for 90° and 180° diameter FOV cameras shown in **Figure 3-1**. We require detection of the reference target at an altitude  $h = 200$  km and  $\rho = 600$  km (see **Figure 2-2**), for which the visual magnitude is  $m_v = 7.2$ . We find that a 3.0 mm aperture gives  $SNR > 5$  in 9 one-second frames for objects at the edge of the FOV, and  $SNR > 30$  for objects at zenith. Using the same STELLAR focal plane array as the WFOV, the IFOV is 0.125 degrees and the F/# is 2.0, as fast as is feasible for optical design. The target streak at zenith is 3.7 pixels per frame for an object at zenith in a 200 km altitude circular orbit and 15.1 pixels for an object at zenith in a 50 km altitude circular orbit.

Going from idealized radiometry to actual designs, hemispherical coverage lenses (fisheye) are existing concepts in commercial video and photography, and can be designed for a Lunar mission well. The major limitations of such lenses are substantial distortion and large first lens to entrance pupil ratios. Distortion maps can be performed during ground testing and provided to the onboard algorithms to account for distortion in orbit determination.

In Figure 2-3 we present two potential optical solutions to achieve the required FOV. The first

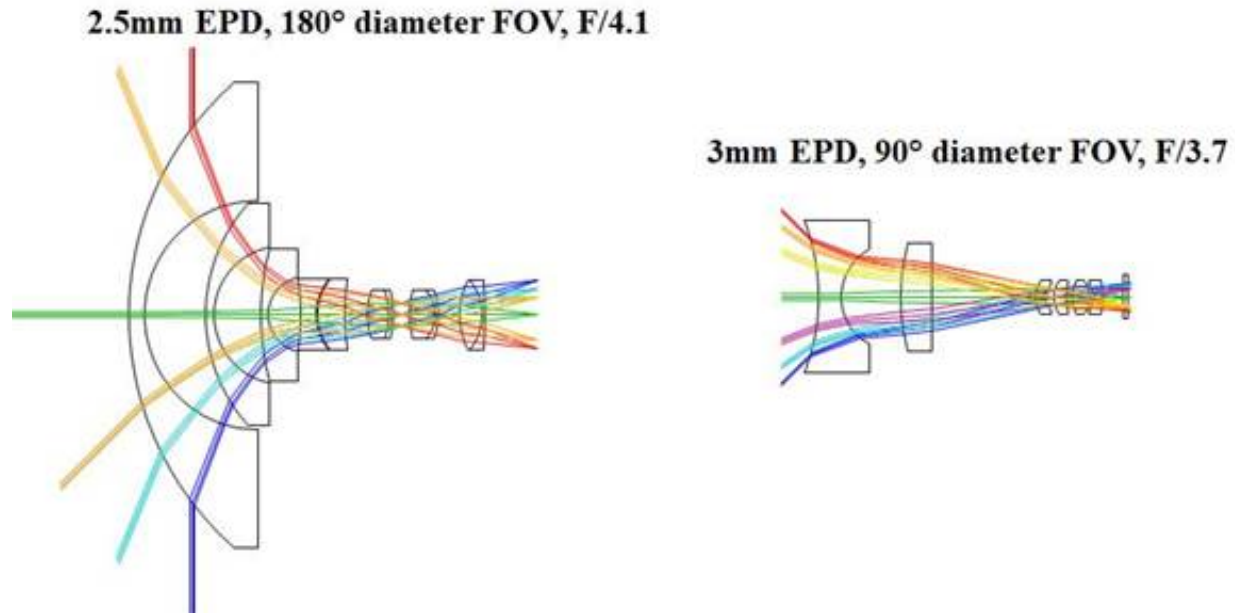


**Figure 2-3: Bounding cases of a FishEye camera. Left: Nikon Patent USPT 3,737,214, FOV covered by one camera. Right: Ball Heritage, FOV covered by 3-4 cameras. EPD = Effective Pupil Diameter.**

### 3 Mission Performance

We examine the performance of the WFOV camera in the LSO instrument suite against the target deck defined by sampling these 480 orbits:

- Periapsis altitudes of 0.02 and 1.0 lunar radii
- Apoapsis altitudes of 0.02, 1, and 5 lunar radii
  - 0-, 10-, 80-, and 90-degree inclinations
- Periapses at N and S poles
- RAANs of 0, 90, 180, and 270 degrees
- Orbital phases in 1/6<sup>th</sup> period intervals over half a period

The simulation length was one year. The merit function for a network is the average over all orbits of

$$M = \sum W_i \cdot \text{numAccess}_i \cdot \max(\text{meanAccessTime}_i / \text{revisitTime}, 1)$$

where  $W$  is a weight defined by a notion of which orbits are the most important,  $\text{numAccess}$  is the number of accesses, an access is a continuous direct line of sight between the observer on Moon and at a target in orbit *when the Moon station is available*,  $i$  is the orbit index, and the revisit time is 22 min as discussed above. That is, if the target is in the FOR for less than the revisit time there is still a chance it will be seen, while if it is in the FOR for more than a revisit time it will certainly be seen. A Moon station is available if it instantaneously has both power and comm link to Earth, which is determined by the power source (solar/nuclear) and comm architecture (DWE/relay). Future studies will examine batteries for limited night operation, and store-and-forward data links for limited relay outages.

The weights  $W$  are:

- Basic value of 1 point
- +1 point for periapse  $\leq 0.05$  lunar radii. These orbits will be used for landing and surface observation
- +1 point for inclination  $\geq 80$  degrees and periapse near N. Pole. There's water at the N. Pole but not as much as the S. Pole.
- +2 points for inclination  $\geq 80$  degrees and periapse near S. Pole, the locus of human activity through 2035.

The revisit time for WFOV is 22 minutes and for FishEye – which stares at zenith continuously – the “revisit time” is simply the dwell time, or 5.0 s. All 5 stations have the same observing cadence in this study. We leave the detailed modeling of Farside station operations, in which dark cone searches are interleaved with all-sky observations, for a future paper.

In the next Section, we present summaries of the observer sets and results, followed by tables and discussion comparing the cases.

### 3.1 Case Summaries

#### 3.1.1 Five Site Nuclear Power and Comm Relay

The LSO network has a WFOV camera with Farside comm relays in both N and S NRHOs and a nuclear power source, so that Observatories have power and downlink all the time. The comm relay network is approximated as 100% available for polar and Farside stations.

The WFOV does not work well detecting targets in low altitude (34.7 km) orbits, as they are moving underneath the FOR cones of the observers as suggested in §2.5. When they do intersect the search cones, it's only for about 3 minutes. The higher altitude orbits work better, providing lots of passes that are >22 min. For polar stations, orbits at 34.7 km altitude become unobservable when the inclination is less than 87 degrees, and for equatorial stations these low orbits are detectable only when the sub-target longitude at the Equator is within 3 degrees of the longitude of the station. Unlike polar stations, however, equatorial stations will still detect low targets at arbitrary RAAN and inclination during one or two 12 h windows per month, as the Moon's rotation brings the target into view during daylight. Two windows occur per month when flyovers are near twilight, in which case the target is illuminated while the ground station does not have to be.

#### 3.1.2 Five Site Solar Power and Comm Relay

The LSO network has a WFOV camera with Farside comm relays in both N and S NRHOs and is solar-powered. The comm relay network is approximated as 100% available for polar and Farside stations as in Section 3.1.1. Each node is functional only when the Sun is above the topographic horizon. For peaks near the poles, we approximate the topo horizon as 0.84 degrees below the geoid horizontal, derived from matching the average amount of light at the topo location [19] to that of a sinusoid with an amplitude equal to the obliquity of the lunar equator to the ecliptic and an offset equal to the topo horizon depression. Equatorial sites would not function half the month while polar sites would have a complex series of topography-dependent outages during the local lunar winter.

We get the same results for WFOV detections of targets in low altitude orbits as in 3.1.1, except that equatorial stations detect low-flying targets in only the daytime 12 h window once per month, as the station does not function when the Sun is down.

#### 3.1.3 Station 1: Initial Operating Capability (IOC) at the South Pole

The LSO "Network" has a WFOV camera at a single station, "Station 1," which establishes IOC with an Observatory on the rim of Shackleton Crater. At first, comm is DWE but is soon upgraded to ~100% relay service either through the Lunar Gateway [2] or LunaNet [16], which have about the same comm coverage for the S. Pole. Thus Station 1 can be built, and IOC can be established as early as possible without waiting for a comm relay, but when activity at Shackleton is high enough to require a comm relay for other purposes Station 1 can then double its effectiveness by observing and transmitting while Earth is below the horizon. The same polar topographic horizon criterion as Section 3.1.2 is applied to power operability. We also looked at the merit of Station 1 with a FishEye camera, with relay, and added the merit of WFOV and FishEye to approximate the merit of Station 1 with both cameras, since few targets are observed by both WFOV and FishEye simultaneously.

### 3.2 Mission Analysis Summaries

**Table 3-1: Merit and Max Outage results for various LSO networks.**

Network	Mean merit	Max Outage (h)
S. pole, solar, DWE	1.5	348
S. Pole, solar, relay (Station 1)	3.0	~150
S. Pole, solar, relay (Station 1) + FishEye	5.4	~150
S. Pole, nuclear, relay	3.9	4
5 stations, solar, relay	12.8	See Table 3-2
5 stations, nuclear, relay	25.0	See Table 3-2

The S. Polar max solar outages are from the site-specific data in [19] rather than the sinusoidal approximation used to calculate merit, while the maximum relay outage is set by for Gateway (S. Pole only) or LunaNet (global). For the 5 station networks, mean availability and maximum outages vary by station as shown in Table 3-2, with same bounds.

**Table 3-2: Availability and Outages of Individual Stations. S = Solar, N = Nuclear, R = Relay**

	Mean Availability				Maximum outage (h)			
	S-DWE	S-R	N-DWE	N-R	S-DWE	S-R	N-DWE	N-R
N	36%	70%	49%	100%	354	150	354	4
S	34%	71%	45%	100%	354	150	354	4
E	51%	51%	100%	100%	354	354	0	0
W	50%	50%	100%	100%	354	354	0	0
F	0%	49%	0%	100%	$\infty$	354	$\infty$	4

Table 3-2 was derived from JPL HORIZONS ephemerides for Earth/Sun elevations above the lunar geoid (no local topography), for the station coordinates in Section 2.1.3, for a year commencing 2/7/2025. The table shows that without nuclear power, there will be ~150 h gaps for individual polar stations. This gap could also be reduced with advanced solar power concepts such as masts, mobility, or beamed power or cables from nearby lit regions of the same topographic high [19]. However, at least one station in the 5 station network will function all the time except for the solar/DWE network, which will suffer gaps up to 114 h during which no stations are operating.

### 3.3 FishEye has High Marginal Value

The FishEye merit function is 77% of that of the WFOV for the Station 1 mission. Even with the smaller range (600 km) of FishEye, this is no surprise since our merit function heavily weights low-flying targets near the S. Pole in the belief that the S. Pole will be the locus of human activity in the near future. Given the infrastructure need to support WFOV (Section 4) already, the marginal value of FishEye will be high.

Fisheye will also keep a continuous eye on a cone above Shackleton Crater, detecting 1.0 m objects moving at ~2.0 km/s at altitudes as low as 5 km, and detecting slower-moving objects either landing or taking off as they pass nearby.

## 4 Eyes on the Sky over Shackleton Crater

### 4.1 Overview: Making the Cameras work on the Lunar Surface

In this section, we will take our two cameras – WFOV and FishEye – and develop a detailed strawman concept of how they would work on the lunar surface, integrated with the Observatory bus.

### 4.2 Pointing

The WFOV camera has to be placed on a 2-axis gimbal assembly to provide the FOV needed for the LSO mission. COTS actuators are controlled using a COTS pointing electronics that provide 0.02 deg pointing accuracy and 5  $\mu$ rad point stability. This step and scan systems provides +/-23.5° az and el movement up to using flex cables, or up to +/-120° with twist capsules. For added flexibility, tables can be updated to vary scan patterns and dwell times as required.

### 4.3 Mission Data Processing (MDP) Enables a Lunar Communication Solution

Since the Moon is 9x further way from the Earth than GEO, data is 81x more difficult to transmit. Users accustomed to >20 Mbps data rates must consider how to best use ~300 kbps typical of NASA CLPS suites, or invest a great deal of money in both on the spacecraft and in the ground stations (as did Mars Reconnaissance Orbiter) to achieve high data rates at lunar and planetary distance. Faced with a similar problem, the *Kepler* planet-detection mission [17] collected for each target a cluster of pixels each of which was predicted to exceed an SNR threshold. This set of pixels was called the “optimal aperture” and aperture shapes were informed by SNR modeling of the data and not defined as rectangles by fiat. A “halo” of pixels was added around the optimal aperture to informed more sophisticated ground-based processing of the transmitted pixel data. However, *Kepler* and *K2* [18] showed that halos are very expensive in pixels for faint sources with small optimal apertures – for example, a 2x2 aperture would expand to a 4x4 aperture, quadrupling the number of pixels collected, for a single-pixel halo. As applied to LSO, the pixels which exceed a data-derived threshold are clustered into apertures based on the data collected. Apertures would be long and thin and

oriented at some angle to the focal plane axes for streaked targets. The aperture can be processed on-board to extract an “detection” – the zeroth, first, and second moments of the pixels in the aperture, which are equivalent to flux, centroid, and streak length/width/orientation angle. Detections can be further filtered to have interesting (non-stellar) moments. Finally, the MDP could identify only detections which persist on multiple frames in a manner consistent with being a resident space object; these data are called “observations.” On the other hand, users often prefer to have the rawest possible data for algorithm development and understanding false positive/false negatives. The solution is to switch MDP between various levels depending on mission phase and downlink available, with example values from synthetic images of the North Ecliptic Pole (NEP):

- Level 0: Full image, 15 Mbps.
- Level 0.5: Median-filtered stack of 5 frames, 3 Mbps. Median filtering removes cosmic rays.
- Level 1: Exceedance pixels only. Most of the sky is noise, a threshold of 5x median noise reduces data volume by 35x to 400 kbps, close to the PRISM-CLPS downlink allocation. This reduction depends on the threshold, location on the sky, and image boresight motion with respect to inertial.
- Level 2: Detections with interesting moments, allocated as 100 detections of 480 bits each plus some header info = 40 kbps. The 480 bits may be thought of as 32 bits for a target ID and each of 6 moments, with margin.
- Level 3: Observations, also 40 kbps.

Since faint moving targets can be missed by the thresholding, a Velocity-Matched Filter (VMF) can be enabled to separate moving objects from stars and collect halo pixels while greatly reducing the number of pixels and detections downlinked. Real-time VMF for 1 Hz, 1024<sup>2</sup> images is Technology Readiness Level (TRL) 7 at Ball.

#### 4.4 Mass

It is important to note that the above referenced hardware designs have been optimized for recurring costs for space-based missions. Design trades to optimize and lightweight designs will be required for LSO mission because the main cost driver is the delivery of mass to the lunar surface. Potential light weighting solutions include trading aluminum structure for composite and/or titanium structure, reducing optical count while tightening alignment requirements to maintain sensitivity and angular accuracy, and investigation 3D printed flexors vs. traditional manufacturing costs. These trade may increase manufacturing and integration costs, but will reduce overall system costs due to delivery costs mass reductions.

As a point of reference, the mass allocation is the same as that for the PRISM instrument suite, 50 kg total for all instruments. We allocate 30 kg to observatory bus functions not included in lander services.

#### 4.5 Solar Power on Peaks of Persistent Light

To find auspicious places for Station 1, we sorted Table 4 [19] by time-weighted illumination percentage over a 0.01 km<sup>2</sup> region. One of the best sites [19] was S28 at longitude 196.7 latitude -89.685, with a 68% illumination percentage and the minimum maximum period in shadow of 147 h, which we used for Station 1. The actual illumination during winter will depend on the topography on the scale of the lander within the 0.01 km<sup>2</sup> parcel; for robustness, the solar panels are affixed to a 2-3 m boom on the top of the lander to rise above meter-scale obstacles.

The amount of power required for the instrument suite is 150 W, as for PRISM [8] with an equal allocation to the observatory bus functions. The total of 300 W will then require about 1.5 m<sup>2</sup> of solar panel, oriented vertically.

#### 4.6 Dust

As noted by Eugene Cernan, commander of Apollo 17, lunar dust is “one of the most aggravating, restricting facets of lunar surface exploration sticking to everything, including metals, skin, spacesuit materials.” Problems cause by lunar dust include:

- Reduced efficiency of solar arrays
- Degraded performance of radiative surfaces
- Premature wear out of mechanisms
- Decreased sensitivity of optical systems
- Degradation of vacuum seals
- Silicosis in human lungs (particles are very small and sharp)

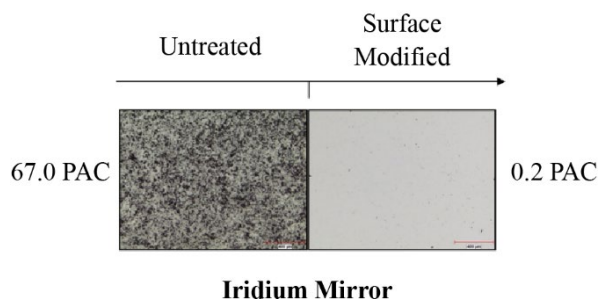


**Figure 4-1: Ball’s STAR treatment reduces Percent Area Coverage (PAC) of lunar dust simulant.**

For LSO, dust on optical surfaces would be mitigated based on a combination of Electrodynamic Shields (EDS) pioneered at Kennedy Space Center [20] and Ball's Surface Treatment Adhesion Reduction (STAR) process [21]. Dust in the gimbal mechanism would be mitigated by labyrinths based on Ball's L-CIRiS lunar thermal camera azimuth gimbal design.

#### 4.7 Thermal

Although polar and equatorial location on the Moon exhibit very different thermal environments, what they share in common are heat fluxes varying gradually over the course of a lunar day, and peaking at lunar noon. Accordingly the thermal control system of polar and equatorial observatories maintain some common design features. Central to that design is a horizontal skyward-facing radiator penetrated by the WFOV sensor and telescope baffle. Sensor components (detector, telescope, rotation assemblies) and electronics maintain thermal contact with the radiator through bolted interfaces and thermal straps. Components, including the radiator itself, are under closed loop temperature control for observatory operations during the lunar day. After sunset, instrument temperature drops towards the lower survival temperature limit, activating an independent thermostatic control system for the radiator that maintains the observatory within its survival temperature range throughout the night.

Maximum required heater power scales with radiator area. Required heater power, and radiator area, is greater for equatorial observatories than for polar ones. Preliminary calculations for one site near the S. Pole indicate that an observatory may operate with < 20 W heater power and < 500 cm<sup>2</sup> radiator area. Margin in these values is advisable due to several uncertainties: surface albedo variations, intermittent shadowing from topographic features and the extent of dust deposited on radiators during landing, thereby reducing radiator emissivity. Thermal design must also take account of the lander and its interfaces, especially mounting location on the lander, the reflective and emissivity properties of lander surfaces, and potentially the presence of other nearby payloads .

## 5 Station 1 Observatory: Payloads and Partners

### 5.1 Suitemates

Lunar SDA observatories would play a valuable role with an instrument suite which also includes sensors which monitor the lunar environment for variables affecting the safety of personnel, facilities, and persistent operations. A seismometer, or system of seismometers would be an especially effective complement to an observatory, enabling the detection of impact signals from meteors, space debris and other falling objects. Seismometers on several Apollo missions demonstrated that impacts are clearly detectable in the seismometer signal [22]. The sensitivity of spaceborne seismometers has improved since the Apollo missions [23], to levels now capable of detecting impacts of lower energy, just sufficient to threaten buildings or space-suited astronauts. Correlating observatory and seismometer measurements will enable real-time assessments of the danger posed by objects in very low orbit by determining whether a spaceborne object has already fallen to the surface, or remains a danger for future impact.

Candidate instruments of other types that would support the environmental monitoring include:

**Radiation sensors for time-resolved radiation levels:** A dosimeter would measure the level of solar particle events and galactic cosmic rays that constitute the primary dose source for astronauts. Upwelling neutrons and gamma rays also contribute to dose [24] and could be measured by appropriate detectors. Examples include GOES-R Solar and Galactic Proton Sensor (SGPS), the NASA PRISM Gruithuisen Dome environmental science/biological monitoring package, and the Chang'e 4 LLND instrument [25]

**Dust detection and characterization:** Lunar dust measurements of relevance to safety of personnel and instruments include dust density and its variation with time, charge state, and particle size distribution over the micron and submicron range [26]. Dust transport can be characterized by sensors utilizing deflecting electrodes to measure the charge, mass, and velocity of dust in motion [27] or by camera to image lofting dust directly [28].

**Surface temperature:** Lunar surface temperature is a key variable for human and automated lunar operations, with potential gradients as large as 100 K in the space of centimeters from shadow to illuminated regions [29]. Radiometric imaging from a thermal infrared camera on a rotating stage provides a means of continuous thermal mapping of surroundings [30].

Instruments which might enhance a general sense of awareness include:

- RF Direction Finder (DF), 2-30 GHz, phased array of dual-polarization sinuous antenna for traffic location
- Laser cornercube for geodesy – entirely passive, but very valuable for knowing exactly where things are
- Navigation beacon

## 5.2 Sharing the Ride Safely

Several lunar landers have payload capacities several times larger than the 50 kg allocated to the instrument suite. This capacity is sold to other government agencies and commercial customers. While in some sense it is desirable for LSO to have a lander to itself, there will be more flight opportunities at lower cost per kg if LSO is willing to share a ride with other customers on a bigger lander. An analogous case is flying an SDA payload on a foreign spacecraft; the Air Force has done this in an arrangement with Japan [33]. Security concerns are addressed by an encryptor card to decrypt commands and encrypt data, as Ball has done in other programs.

## 5.3 Lander Interface and Accommodation

NASA is presently implementing a plan for regular payload delivery to selected lunar locations as part of the Commercial Lander Payload Services (CLPS) program [7]. Although the program supports lander development by multiple commercial providers, a common set of interface guidelines has been promulgated. Preliminary SDA observatory design complies with these guidelines. Command and data communication is by means of RS-422 electrical interfaces. Power is sourced from the lander through two separate 28 V supplies, one for payload operation and one for thermal control. The thermal interface to the lander is adiabatic

Preliminary observatory design makes upfront assumptions about where to implement functions that may be resident in the lander, payload, or shared between the two. The observatory maintains its own thermal control (Section 4.8), utilizing heater power provided by the lander. Some details of the design, particularly radiator configuration and size, are dependent on mounting location on the lander, and lander properties. Observatory electronics include 4 Gb (TBR) nonvolatile flash memory for storage of observatory data, up to one day of Level 2 or 3 data (§4.3). Data is transmitted at regular intervals to lander memory for subsequent downlinking to the Earth. Lander software issues commands to the observatory for data transmittal and other functions, including regular automated commands as well as specialized commands relayed from the MOC.

# 6 Conclusions

## 6.1 Gross Assessment of Performance vs. Cost

Mission modeling shows that the “5 site, nuclear, relay” network is about 2.1x as effective as “5-site, solar, relay” which is not surprising since the Sun is above the horizon roughly half the time. This conclusion is robust not just for WFOV and FishEye, but for every instrument suite, since for the solar-powered stations nothing works at night and all instruments work during the day. However, some simple math suggests that the total cost (including delivery) of an RTG-powered observatory might be about 4x that of a solar observatory:

1. Taking the PRISM instrument suite allocations of 50 kg, 150 W, and 30 M\$, the total cost of a PRISM suite including freight would be 90 M\$. This could double with modifications for persistence, as happened with NASA’s VIPER rover, to \$180 M.
2. RTGs have two high costs: the cost to build it, and the cost to land it on the lunar surface. Using \$1.0 M/We and 2.3 We/kg as the specific cost and power, and assuming that the observatory bus uses the same amount of power as the instrument suite, we find the delivered cost of the RTG alone is \$420M for 300 W, for a total of \$510M when added to the instrument suite.

In addition, it is not at all clear that the US could produce that many RTGs even if they were cost-effective; the DOE-NASA Pu-238 pipeline produces one 100 We MMRTG unit per year, possibly two with upgrades [31], which would be allocated to planetary exploration as well as SDA. It would be more effective and less risky to build 2x as many solar observatories and distribute them in longitude around the Moon. Even though half are off-line at any given time, an object in orbit around the Moon will pass over a sunlit side (or at least the terminator) at least once in its orbit. Finally, even at the same level of cost-effectiveness the smaller dollar value might be easier to fund.

## 6.2 Feasibility

The instrument suite and delivery system are in-family with that being developed by NASA for CLPS and PRISM. Other features, such as multi-night survival and Farside comm, have been demonstrated by China in the last few years and ought not be beyond the technical abilities of the US in the near future if persistent efforts are made. A survival example is NASA’s VIPER rover, which will explore permanently shadowed regions for volatiles for several months. A comm example is NASA’s Lunar Gateway, which is under construction and will be launched in 2024, providing an effective relay capability for S. Polar sites.

### 6.3 Recommendations

These initial studies lead us to recommend:

- Solar power over nuclear (RTG) power. This is true even for a single S. Polar station, in which case it would be cheaper to land two Observatories a few km from each other on opposite sides of a polar peak instead of building a single nuclear-powered station.
- A 5-station network, with IOC of an observatory on the rim of Shackleton crater
- Use the NASA Gateway for IOC and LunaNet for all-Moon all-the-time access, perhaps on a subscription basis rather than having to build, own, and operate the relay system.
- A Wide Field of View and a FishEye camera

We suggest future studies which:

- Compare LSO to lunar orbit SDA effectiveness (see companion paper [1])
- Trade cost vs. weight
- Identify instrument suitemates
- Build instruments on the ground for prompt use as rides become available (NASA CLPS and PRISM model)
- Investigate beamed power for polar sites, to a level of fidelity where the specific cost in \$/W can be compared to RTGs.

## 7 Acknowledgements

Dr. Jeffrey E. Van Cleve contributed paper integration, radiometry of WFOV and FishEye, stray light calculations, and lunar science and mapping expertise. Dr. David P. Osterman contributed an analysis of the thermal environment and thermal control, and the list of candidate instruments to monitor the lunar environment of each observatory. Dr. Jacob D. Griesbach conducted the mission and performance access modeling and simulations. Anna Lawitzke contributed her expertise in the CT-2020 star tracker family development, and in lunar dust science. Emily MacAnlis provided additional WFOV camera technical information and general paper review. Elvis Silva, an Advanced Systems Manager, is focused on the development of concepts of cislunar space domain awareness and architectures that are of relevance to the domain. Chris Grant, an Advanced Systems Manager, leads Ball's long-range concept development for Space Domain Awareness. Amelia Bloom contributed the mission data processing concept and is an expert in SDA algorithm development. Dr. Melissa Sampson contributed her expertise in commercial space and lunar development, in particular CLPS vendors and lander technology development.

We also acknowledge Jim Contreras for the CT-2020 and FishEye optics. This work was funded by Ball internal funds.

## 8 References

- [1] E. Silva, J. Van Cleve, R. Philbrick et al., System and Methods for Hybrid Lunar Surface and Space Domain Situational Awareness, *AMOS 2021*
- [2] R. Whitley and R. Martinez. Options for Staging Orbits in Cis-Lunar Space. *2016 IEEE Aerospace Conference*, 2016.
- [3] A. Greynolds. Formulas For Estimating Stray-Radiation Levels In Well-Baffled Optical Systems. *Proc. SPIE 0257, Radiation Scattering in Optical Systems*, 1981
- [4] [http://www.ctio.noao.edu/telescopes/opteng/DMO\\_info.html](http://www.ctio.noao.edu/telescopes/opteng/DMO_info.html)
- [5] D. Schroeder, *Astronomical Optics*, 1<sup>st</sup> Edition, 1991
- [6] K. Krisciunas and B. Schaefer. A Model of the Brightness of Moonlight. *Publications of the Astronomical Society of the Pacific*, 103:1033-1039, 1991
- [7] <https://www.nasa.gov/content/commercial-lunar-payload-services>
- [8] NASA Research Opportunities In Space And Earth Sciences – 2021 (ROSES-2021) Amendment 22: Payloads and Research Investigations on the Surface of the Moon (PRISM)
- [9] <https://www.astrobot.com/>
- [10] <https://www.spacex.com/media/Capabilities&Services.pdf>
- [11] [https://mars.nasa.gov/files/mep/MMRTG\\_Jan2008.pdf](https://mars.nasa.gov/files/mep/MMRTG_Jan2008.pdf)
- [12] Cost Comparison in 2015 Dollars for Radioisotope Power Systems -- Cassini and Mars Science Laboratory <https://www.osti.gov/biblio/1364515>
- [13] [https://www.nasa.gov/directorates/spacetech/niac/2021\\_Phase\\_I/Light\\_Bender/](https://www.nasa.gov/directorates/spacetech/niac/2021_Phase_I/Light_Bender/)

- [14] H. Chu, L. Ma, K. Wang et al., Trajectory optimization for lunar soft landing with complex constraints, *Advances in Space Research* 60: 2060–2076, 2017
- [15] <https://heasarc.gsfc.nasa.gov/docs/tess/the-tess-space-telescope.html>
- [16] Lunar Communications Relay and Navigation Services (LunaNet) <https://sam.gov/opp/8116f285e8d841a6a5e030c00fb7fa76/view>
- [17] Kepler Instrument Handbook [https://stdatu.stsci.edu/files/live/sites/mast/files/home/missions-and-data/kepler/\\_documents/KSCI-19033-002-instrument-hb.pdf](https://stdatu.stsci.edu/files/live/sites/mast/files/home/missions-and-data/kepler/_documents/KSCI-19033-002-instrument-hb.pdf)
- [18] KSCI-19116-003: K2 Handbook [https://stdatu.stsci.edu/files/live/sites/mast/files/home/missions-and-data/k2/\\_documents/KSCI-19116-003.pdf](https://stdatu.stsci.edu/files/live/sites/mast/files/home/missions-and-data/k2/_documents/KSCI-19116-003.pdf)
- [19] E. J. Speyerer and M. S. Robinson. Persistently illuminated regions at the lunar poles: Ideal sites for future exploration, *Icarus*, 222:122–136, 2013.
- [20] P. J. Mackey, M. R. Johansen, R. C. Olsen et al. “Electrodynamic Dust Shield for space applications,” *ASCE Earth and Space Conference*, Orlando, FL, 2016
- [21] G. Devaud, C. Haley, C. Rockwell, and A. Fischer. Surfaces that shed dust: unraveling the mechanisms. *Systems Contamination: Prediction, Measurement, and Control*, vol. 9196, p. 919603, 2014.
- [22] P. Lognonné, M. Le Feuvre, C. L. Johnson, and R. C. Weber. Moon meteoritic seismic hum: Steady state prediction, *Journal of Geophysical research, Planets*, 114 E12, 2009
- [23] P. Lognonné, W. B. Banerdt, D. Giardini et al. SEIS: Insight’s Seismic Experiment for Internal Structure of Mars. *Space Sci Rev* 215, 12 (2019). <https://doi.org/10.1007/s11214-018-0574-6>
- [24] J. H. Adams, M. Bhattacharya, Z. W. Lin et al. (2007). The ionizing radiation environment on the moon. *Advances in Space Research*, 40, 338-341.
- [25] S. Zhang, R. F. Wimmer-Schweingruber, J. Yu et al. First measurements of the radiation dose on the lunar surface. *Science Advances*, 6:eaaaz1334. 2020
- [26] E. Grun, M. Horanyi, Z. Sternovsky, The Lunar Dust Environment, *Planetary and Space Sciences*, 59, 14, 2011, 1672-1680
- [27] X. Wang, Z. Sternovsky, and M. Horanyi et al., Cubesat electrostatic dust analyzer (CEDA) for exploring dust transport processes on airless planetary bodies. *49th LPSC conference*, paper 1755, 2018
- [28] N. Hood, A. Carroll, R. Mike et al., Laboratory Investigation of Rate of Electrostatic Dust Lofting Over Time on Airless Planetary Bodies, *Geophysical Research Letters*, 45, 24 2018.
- [29] P. O. Hayne, O. Aharonson, and N. Schörghofer. Micro Cold Traps on the Moon. *Nature Astronomy*, 5:169-175, 2021.
- [30] P. O. Hayne, D. P. Osterman, K. Donaldson-Hanna, and D. A. Paige. A Compact Instrument for Mineralogical and Thermophysical Studies of the Moon from the Lunar Surface. AGU Fall Meeting, abstract #P31C-3444, 2019
- [31] [https://www.lpi.usra.edu/opag/march\\_08\\_meeting/presentations/dudzinski.pdf](https://www.lpi.usra.edu/opag/march_08_meeting/presentations/dudzinski.pdf)
- [32] P. Jenniskens, R. Dissly, I. D. Boyd et al. ASIMA - Asteroid Impact Analyzer: A proposed close-to-home planetary mission to probe the diversity of comets and asteroids. *40th LPSC conference*, paper 2305, 2009
- [33] <https://www.spaceforce.mil/News/Article/2451728/japans-office-of-national-space-policy-signs-historic-mou-with-the-us-space-for/>